

A NEW METHOD TO DETERMINE THE TEMPERATURE OF CMES USING A CORONAGRAPH FILTER SYSTEM

KYUHYOUN CHO¹, JONGCHUL CHAE¹, EUN-KYUNG LIM², KYUNG-SUK CHO^{2, 3}, SU-CHAN BONG^{2, 3}, AND HEESU YANG¹

¹Department of Physics and Astronomy, Seoul National University, Gwanak-gu, Seoul 151742, Korea
chokh@astro.snu.ac.kr

²Korea Astronomy and Space Science Institute, 776 Daedeokdae-ro, Yuseong-gu, Daejeon 305348, Korea

³University of Science and Technology, 217 Gajeong-ro, Yuseong-gu, Daejeon 305350, Korea

Received February 30, 2014; accepted February 31, 2014

Abstract: The coronagraph is an instrument enables the investigation of faint features in the vicinity of the Sun, particularly coronal mass ejections (CMEs). So far coronagraphic observations have been mainly used to determine the geometric and kinematic parameters of CMEs. Here, we introduce a new method for the determination of CME temperature using a two filter (4025 Å and 3934 Å) coronagraph system. The thermal motion of free electrons in CMEs broadens the absorption lines in the optical spectra that are produced by the Thomson scattering of visible light originating in the photosphere, which affects the intensity ratio at two different wavelengths. Thus the CME temperature can be inferred from the intensity ratio measured by the two filter coronagraph system. We demonstrate the method by invoking the graduated cylindrical shell (GCS) model for the 3 dimensional CME density distribution and discuss its significance.

Key words: Sun: coronal mass ejections (CMEs) — method: numerical

1. INTRODUCTION

The coronagraph is an instrument to observe the faint structure outside the solar disk. By screening intense radiation from the solar disk, it enables us to observe the K-corona, streamers, coronal mass ejections (CMEs), and other phenomena in the corona. The origin of visible light detected by coronagraphic observations is Thomson scattered light from the solar photosphere by free electrons in the solar corona; its properties depend on the electron density distribution, the polarization, and the scattering angle.

For decades, our knowledge about CMEs has greatly increased through white light coronagraphic observations. A CME expels huge amounts of plasma from the solar atmosphere and is one of the most energetic events in the heliosphere. Since Tousey (1973) carried out the first CME observation using the OSO-7 coronagraph, succeeding spacecraft coronagraphic observations allowed the investigation of CMEs. Now, it is generally accepted that CMEs have three-part structures (Illing & Hundhausen 1985) and are responsible for changes in space weather that affect interplanetary space and terrestrial magnetism (Baker et al. 2008). A number of statistical studies on angular widths (Howard et al. 1985; St Cyr et al. 2000), velocities (Yashiro et al. 2004), and occurrence latitudes (Hundhausen 1993; Goparswamy et al. 2010) were performed with accumulated coronagraphic observation data. But the derived characteristics of CMEs from coronagraphic observations were limited to mainly geometric and kinematic parameters.

Observational reports of CME temperatures are scarce due to the difficulty of spectroscopic observations of CMEs, which are required for temperature determination. The CME temperature can be inferred either from temperature-sensitive line ratios or from the existence of emission lines of specific formation temperatures. Although the spectral profiles in principle can give us the temperature directly, they do not provide spatial information. One can obtain useful spectra only when the slit position is cospatial with the CMEs. Only a few studies reported CME temperatures using the Ultraviolet Coronagraph Spectrometer (UVCS) on board the Solar and Heliospheric Observatory (SOHO) (Ciaravella et al. 2000; Akmal et al. 2001).

Recently, the technique of differential emission measure (DEM) was used to estimate the CME temperature (Lee et al. 2009; Hannah & Kontar 2013). The Atmospheric Imaging Assembly (AIA) on board the Solar Dynamics Observatory (SDO) or the EUV Imaging Spectrometer (EIS) on board the Hinode can observe CMEs lower in the solar atmosphere at various EUV wavelengths. The different temperature dependence of the EUV filters allows us to estimate the multi-thermal structure of CMEs with the DEM method. This method requires the combination of many EUV filters and has height limitations because the EUV filters are usually dedicated to the solar disk observations.

We introduce a new method for the determination of CME temperature through coronagraphic observations. Our method is very simple and has no spatial limitations compared to previous methods. Reginald et al. (2009) measured the electron temperature of the inner K-corona using filter observation during the total

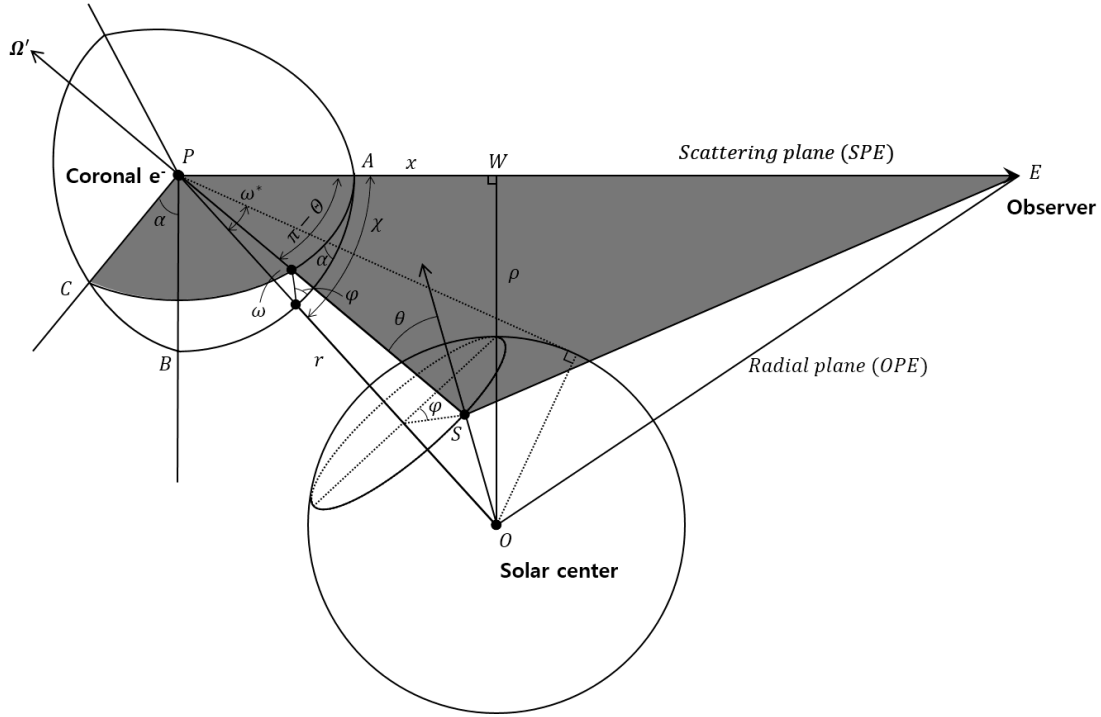


Figure 1. Geometry for the K-coronal spectrum calculation from Reginald (2001).

solar eclipse. We extend this method to the CME temperature measurement using coronagraph filter observations. We consider an isothermal CME with a density structure that is described by a gradual cylindrical shell (GCS) model and calculate the expected filter intensity ratio maps for 4 different CME temperatures using this simple method. We present our results and discuss the importance and the prospects of the method.

2. METHOD AND RESULT

Cram (1976) argued the possibility of coronal temperature measurement from the specific intensity ratio. He noted that strong absorption lines in the visible light irradiated from the solar photosphere are flattened by the Doppler effect from thermal motions of free coronal electrons. High electron temperature flattens the spectrum, and, hence, the intensity ratio between the absorption line center and the continuum decreases. Thus the intensity ratio can be used as an indicator for electron temperature. Since stronger absorption lines are more favorable for measuring the intensity ratio difference, the filters are usually put around 4000 Å where the strongest lines of the Ca II H & K and the G band exist.

Reginald (2001) improved the accuracy of the method by adding the solar wind effect. He supposed that coronal electrons are moving in the radial direction with a constant solar wind speed. In this situation, the light from the solar photosphere appears redshifted to the coronal electrons that are receding from the photosphere. This redshifted light is scattered by the coronal electrons to the observer. If the scattering electron is

positioned behind the solar limb plane, the light is further shifted to the red, enhancing the redshift. On the other hand, if the electron is positioned in front of the solar limb plane, the light is shifted back reducing the redshift (see Figure 3 in Reginald et al. 2009). Thus, the total effect of the solar wind on the scattered light is redshift. It means that a faster solar wind shifts the K-coronal spectrum to longer wavelength and affects the intensity ratio more strongly.

Figure 1 shows the geometry for K coronal spectrum calculation used by Reginald (2001). The light from the solar photosphere (S) is scattered by the free electrons in the corona (P) to the observer (E). For this geometry, Reginald (2001) used the following calculation formula.

$$\begin{aligned} \mathcal{I}_{\lambda}^S(\rho) = & \int_{-\infty}^{\infty} dx N_e(x) \times \\ & \int_0^{2\pi} d\varphi \int_0^{\omega^*} d\omega \sin \omega Q^S(\omega, \varphi) \times \\ & \int_{-\infty}^{\infty} d\lambda' I_{\lambda'}(\omega, \varphi) \frac{1}{2\sqrt{\pi}\Delta b} \times \\ & e^{-[\{\lambda - \lambda'(1 + 2b^2 w \cos \omega/c)\}/(2\Delta b)]^2}. \end{aligned}$$

This equation consists of 4 dimensional integrations. First, the free electrons on each segment (dx) of the line of sight (LOS) contribute to the observable intensity. We should consider the LOS distribution of the free electrons, $N_e(x)$. Reginald (2001) applied the Baumbach model (Baumbach 1937) for the distribution of the K-corona free electrons on the LOS. Second, the

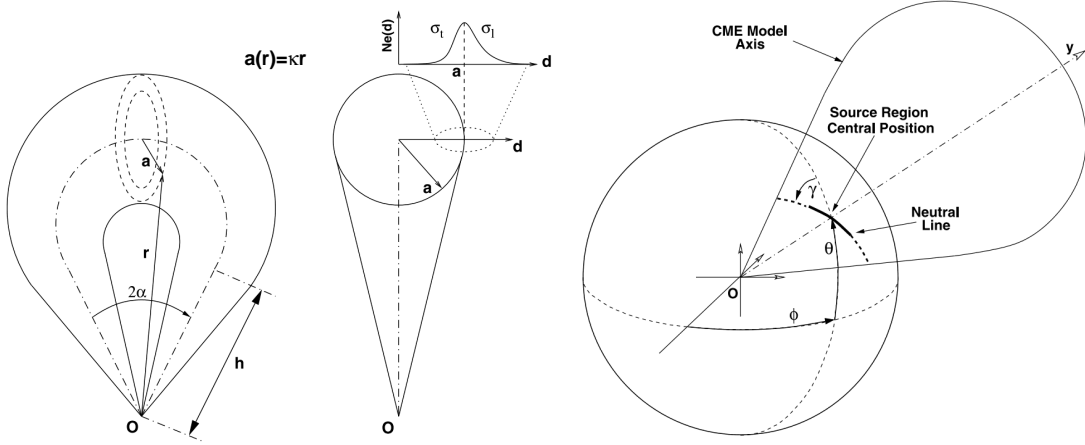


Figure 2. Face-on, edge-on, and 3D representation of the GCS model from Thernisien et al. (2006).

Table 1

Model and Positioning Parameters of the GCS model for 2002 January 4 CME from Thernisien et al. (2006).

| α (deg) | κ | h (R_{\odot}) | n_e (cm^{-3}) | σ_t | σ_l | φ (deg) | θ (deg) | γ (deg) |
|----------------|----------|---------------------|---------------------|------------|------------|-----------------|----------------|----------------|
| 26.9 | 0.43 | 1.48 | 8.69×10^5 | 0.2 | 0.28 | 326 | 25 | 62 |

light is integrated over the solar disk or over the solid angle ($d\varphi d\omega$) of the solar surface spanned by the free electrons (P) in the corona. Limb darkening and polarization are taken into account in this step. Lastly, the wavelength of the incident light ($I_{\lambda'}$) is changed because of the Doppler shift caused by free electron's motion. Reginald (2001) assumed that the main motions for the coronal free electrons are thermal motion of constant K-coronal temperature and constant radial solar wind speed. Thus, the contribution of the Doppler shift of all the motions should be integrated over wavelength ($d\lambda'$). By applying this method, Reginald et al. (2009) obtained the K-coronal temperature map from the total eclipse observation.

The CME spectrum calculation can be conducted using the same method that was used for the K-coronal intensity. This is possible because the emission mechanism is the same for both the K corona and CMEs: Thomson scattering. The geometry, however, is considerably different. A CME is not spherically symmetric as the K-corona. We adopt the GCS model for the 3 dimensional CME density distribution (See Figure 2). Thernisien et al. (2006) tested the GCS modeling technique on 34 LASCO CMEs. Among them, we choose the 2002 January 4 event and adopt their detail parameters for this case study (Thernisien 2010). The adopted parameters are summarized in Table 1. We use a CME speed of 896 km s^{-1} which is recorded in the SOHO/LASCO CME catalog¹. The limb darkening coefficients are extracted from Allen (1973). The extraterrestrial solar spectral irradiance for the incident light from the solar photosphere is provided by Kurucz

(2005)². We calculate the spectra in the vicinity region of the CME with CME temperatures of 0.5, 1.0, 1.5, and $2.0 \times 10^6 \text{ K}$.

From the simulated spectra, we calculate the two filter intensity ratio for every calculated position. To determine the center wavelength of the filters, we simulate the spherically symmetric coronal spectrum and calculate the wavelengths at which the filter intensity ratio change is maximized with respect to the temperature change. From the result, we select the Gaussian filters which have a width of 30 \AA and center of 4025 \AA and 3934 \AA , respectively. These wavelengths are slightly different from 3850 \AA and 4100 \AA used by Reginald et al. (2009), possibly due to differences in the spectrum simulation or wavelength selection method. Finally we obtain a filter intensity ratio between the two filters ($I(4025 \text{ \AA})/I(3934 \text{ \AA})$) for every spatial pixel near the CME.

Figure 3 shows the observed CME image using LASCO C2 (a), the simulated CME image at 4025 \AA (b), and the calculated filter intensity ratio maps with different temperatures (c-f). Note that in each case the temperature is assumed to be uniform over the CME. The filter intensity ratio, however, changes with position, showing higher values at the leg parts of the CME. We conjecture that the non-uniform filter intensity ratio results from the different amount of the Doppler shift due to the asymmetric density structure and height effect. When the scattered light comes from a coronal electron to the observer, the LOS distance between the coronal electron and the solar limb plane determines the amount of the Doppler shift. Therefore, an asymmetric density structure can generate a

¹http://cdaw.gsfc.nasa.gov/CME_list

²<http://Kurucz.harvard.edu/sun/irradiance2005/irradthu.dat>

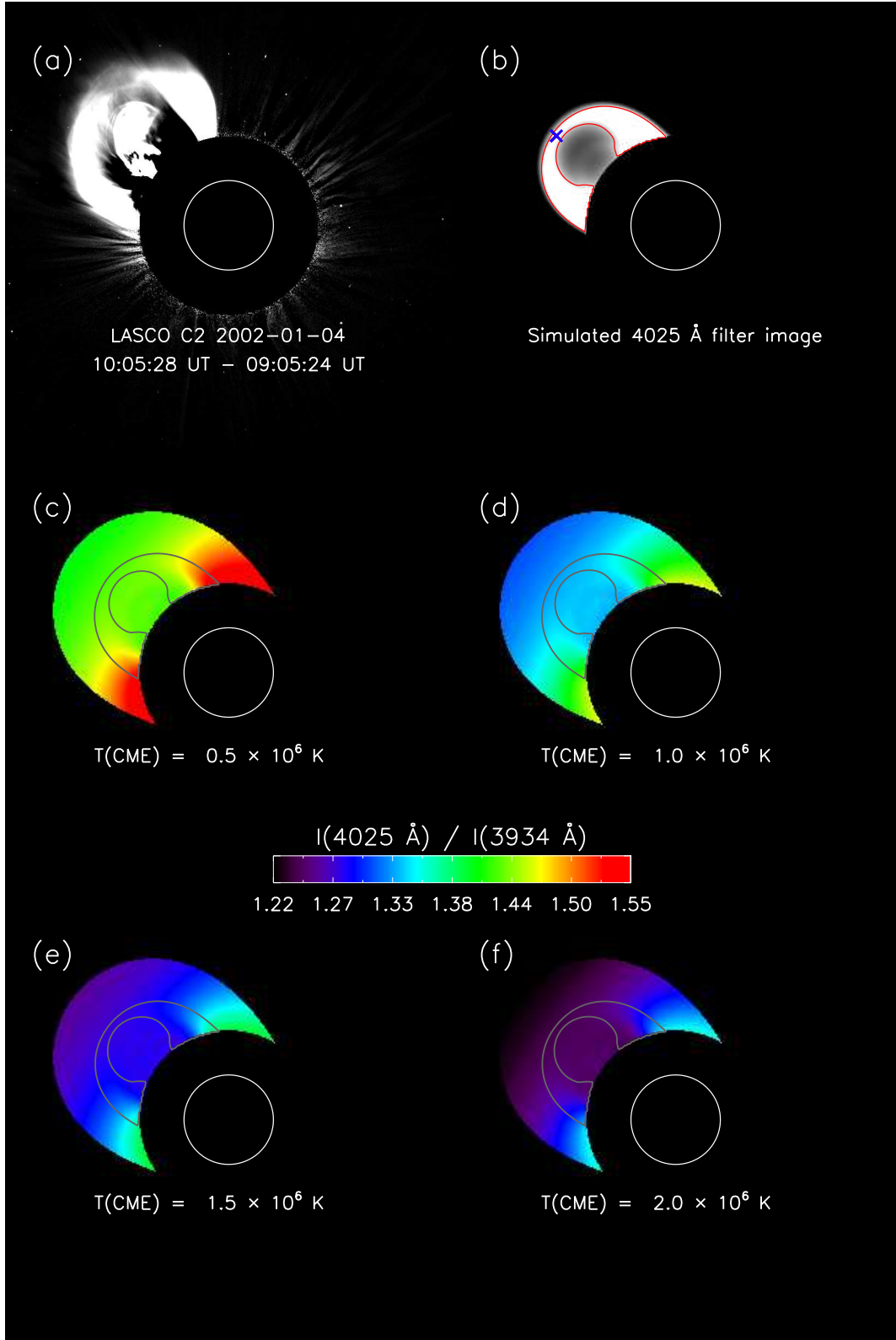


Figure 3. (a) LASCO C2 difference image. (b) simulated 4025 Å filter image. (c)-(f) Calculated two filter intensity ratio images with CME temperature of 0.5 , 1.0 , 1.5 , and 2.0×10^6 K. The gray contours represent the simulated CME structure in Figure 3b.

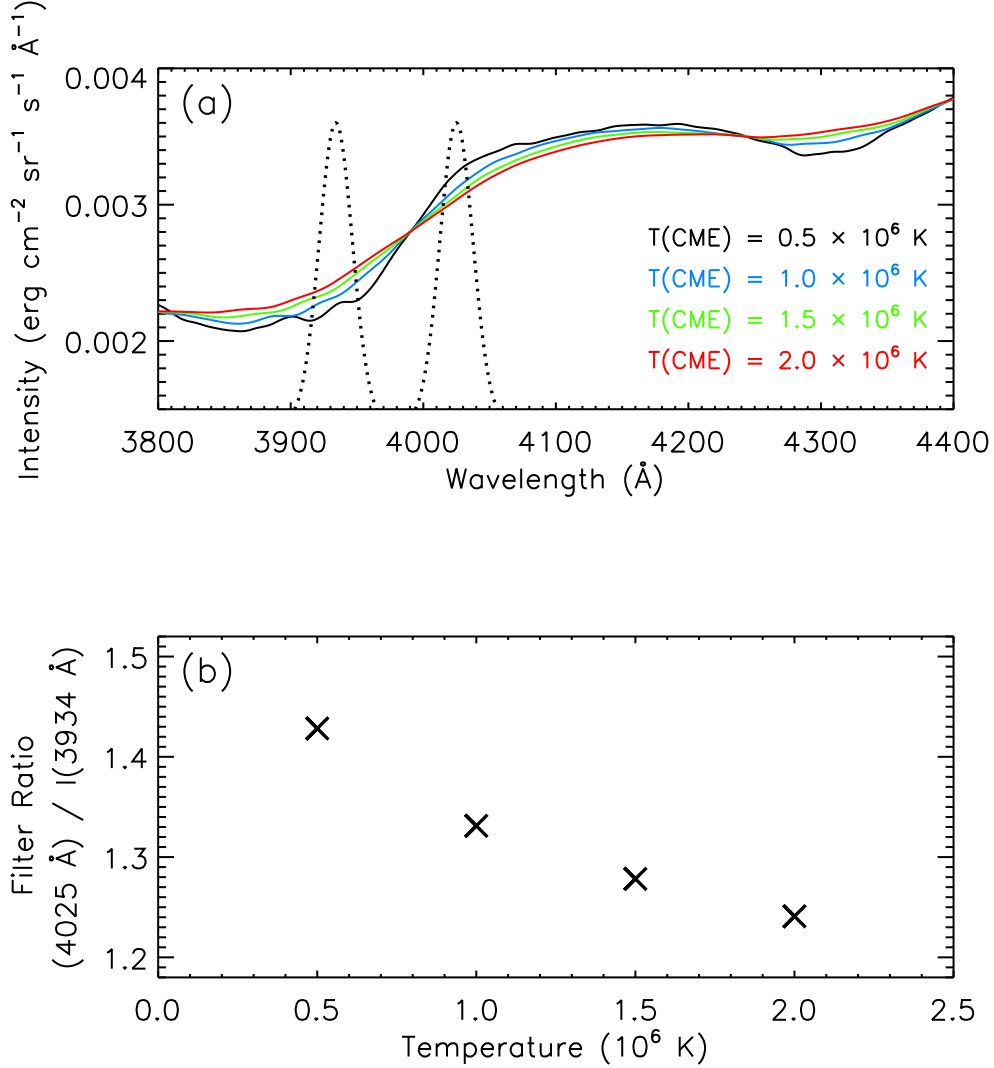


Figure 4. (a) CME spectrum at the blue cross position in Figure 3b with CME temperature of 0.5, 1.0, 1.5, and 2.0 × 10⁶ K. The dashed Gaussian profiles represent filter response functions with centers of 3934 Å and 4025 Å, respectively. (b) Relation between CME temperature and the filter intensity ratio.

non-uniform filter intensity ratio. Height is also related with the Doppler shift. Coronal electrons located at lower heights are less affected by Doppler shift because lots of photospheric radiation has large incidence angle against the radial motion of the CME. Despite this non-uniform filter intensity ratio, Figure 3 clearly indicates that the average filter intensity ratio decreases with the CME temperature.

We focus on the top part of the CME structure (the blue cross position in Figure 3b), which gives the most reliable result because Thernisien et al. (2006) used this position to extract the density parameters (n_e , σ_t , and σ_l) of the CME. Figure 4a shows the simulated spectra for each CME temperature at this position, together with the filter response functions. As Cram (1976) explained, it turns out that higher CME temperature pro-

duces a smoother spectrum. Additionally, we find that the two filters are located at the wavelengths where intensity variation is sensitive to temperature variation.

Figure 4b shows the relationship between CME temperature and filter intensity ratio. The filter intensity ratio varies from 1.43 to 1.24 as temperature increases from 0.5 to 2.0 × 10⁶ K. This anti-correlation is consistent with our expectation. The filter intensity ratio variation is large enough to measure the CME temperature from the observed data, according to Reginald et al. (2009). Even though this variation depends on the assumed CME model, we expect that the model dependence may be weak. This is supported by the fact that the derived variation of filter intensity ratio is found to be comparable to the value obtained by Reginald & Davila (2000) for the spherically sym-

metric K-coronal density distribution. Thus, we expect that the CME temperature is measurable from the filter intensity ratio for a variety of CME models.

3. DISCUSSION

The method of determining CME temperature based on the filter intensity ratio has several advantages over other methods. The biggest one is that it allows temperature determination over a wide field of view, unlike previous spectroscopic observations that had to be confined to a finite number of slit locations. In addition, the observing setup is much simpler than other instruments and can be easily implemented in a coronagraph instrument. It requires only 2 filter images, which is easier to produce than spectrograms or multi-filter images.

In real observations, securing high signal to noise (S/N) is crucial to accurately measure CME temperatures. The filter observations needed for this method have disadvantages compared to current white light coronagraphic observations with respect to the achievable S/N. The filter width (30 Å) is quite narrower than the spectral window of the existing white light coronagraphs (Brueckner et al. 1995; Howard et al. 2008), leading to lower S/N for given exposure time. The problem of low S/N is further exasperated because the waveband for this observation is at near UV wavelengths where the solar irradiance is relatively low and the quantum efficiency of conventional CCDs is low. Thus the instrumental specifications should be considered carefully when acquiring data for the filter intensity ratio method.

We plan to improve the filter intensity ratio method by implementing density distributions other than the GCS model. Because the GCS model considers only 9 free parameters, there are discrepancies between the model and the reality. We confirmed that the filter intensity ratio does not depend on the absolute value of the electron density (n_e) which is the most ambiguous parameter. Verification using other methods is also important. Comparison with results from previous methods or in situ measurements will be a great help in acquiring more reliable results. In the future, we will also investigate the Doppler effect of the CME motion on the filter intensity ratio.

ACKNOWLEDGMENTS

This work was supported by the KASI research fund for Space Weather Forecast Center. LASCO CME catalog is generated and maintained at the CDAW Data Center by NASA and The Catholic University of America in cooperation with the Naval Research Laboratory. SOHO is a project of international cooperation between ESA and NASA.

REFERENCES

- Akmal, A., Raymond, J. C., Vourlidas, A., Thompson, B., Ciaravella, A., Ko, Y.-K., Uzzo, M., & Wu, R. 2001,

- SOHO Observations of a Coronal Mass Ejection, *ApJ*, 553, 922
- Allen, C. W. 1973, *Allen's Astrophysical Quantities*, London, The Athlone Press University of London
- Baker, D. N., Balstad, R., Bodeau, J. M., Cameron, E., Fennell, J. F., Fisher, G. M., Forbes, K. F., Kintner, P. L., Leffler, L. G., Lewis, W. S., Reagan, J. B., Small III, A. A., Stansell, T. A., Strachan Jr. L., Graham, S. J., Fisher, T. M., Swisher, V., & Gruber, C. A. 2008, *Severe Space Weather Events Understanding Societal and Economic Impacts A Workshop Report* (Washington DC: The National Academies Press)
- Baumbach, S. 1937, *Strahlung, Ergiebigkeit und Elektrendichte der Sonnenkorona*, *Astron. Nachrichten*, 263, 120
- Brueckner, G. E., Howard, R. A., Koomen, M. J., Korendyke, C. M., Michels, D. J., Moses, J. D., Socker, D. G., Dere, K. P., Lamy, P. L., Llebaria, A., Bout, M. V., Schwenn, R., Simnett, G. M., Bedford, D. K., & Eyles, C. J. 1995, *The Large Angle Spectroscopic Coronagraph (LASCO)*, *SoPh*, 162, 357
- Ciaravella, A., Raymond, J. C., Thompson, B. J., van Ballegooijen, A., Strachan, L., Li, J., Gardner, L., O'Neal, R., Antonucci, E., Kohl, J., & Noci, G. 2000, *Solar and Heliospheric Observatory Observations of a Helical Coronal Mass Ejection*, *ApJ*, 529, 575
- Cram, L. E. 1976, *Determination of the Temperature of the Solar Corona from the Spectrum of the Electron-Scattering Continuum*, *SoPh*, 48, 3
- Gopalswamy, N., Akiyama, S., Yashiro, S., & Makela, P. 2010, *Coronal Mass Ejections from Sunspot and Non-Sunspot Regions, Magnetic Coupling between the Interior and Atmosphere of the Sun*, eds. S. S. Hasan & R. J. Rutten, *Astrophysics and Space Science Proceedings*, 289
- Hannah, I. G., & Kontar, E. P. 2013, *Multi-Thermal Dynamics and Energetics of a Coronal Mass Ejection in the Low Solar Atmosphere*, *A&A*, 553, A10
- Howard, R. A., Moses, J. D., Vourlidas, A., Newmark, J. S., Socker, D. G., Plunkett, S. P., Korendyke, C. M., Cook, J. W., Hurley, A., Davila, J. M., Thompson, W. T., St Cyr, O. C., Mentzell, E., Mehalick, K., Lemen, J. R., Wuelser, J. P., Duncan, D. W., Tarbell, T. D., Wolfson, C. J., Moore, A., Harrison, R. A., Waltham, N. R., Lang, J., Davis, C. J., Eyles, C. J., Mapson-Menard, H., Simnett, G. M., Halain, J. P., Defise, J. M., Mazy, E., Rochus, P., Mercier, R., Ravet, M. F., Delmotte, F., Auchere, F., Delaboudiniere, J. P., Bothmer, V., Deutsch, W., Wang, D., Rich, N., Cooper, S., Stephens, V., Maahs, G., Baugh, R., McMullin, D., & Carter, T. 2008, *Sun Earth Connection Coronal and Heliospheric Investigation (SECCHI)*, *SSRv*, 136, 67
- Howard, R. A., Sheeley, Jr. N. R., Koomen, M. J., & Michels, D. J. 1985, *Coronal Mass Ejections: 1979-1981*, *J. Geophys. Res.*, 90, 8173
- Hundhausen, A. J. 1993, *Sizes and Locations of Coronal Mass Ejections: SMM Observations From 1980 and 1984-1989*, *J. Geophys. Res.*, 98(A8), 13
- Illing, R. M. E., & Hundhausen, A. J. 1985, *Observation of a Coronal Transient from 1.2 to 6 Solar Radii*, *J. Geophys. Res.*, 90, 275
- Kurucz, R. L. 2005, *New Atlases for Solar Flux, Irradiance, Central Intensity, and Limb Intensity*, *Memorie Della Societa Astronomica Italiana Supplement*, 8, 189
- Lee, J.-Y., Raymond, J. C., Ko, Y.-K., & Kim, K.-S. 2009, *Three-Dimensional Structure and Energy Balance of a*

- Coronal Mass Ejection, *ApJ*, 692, 1271
- Reginald, N. L. 2001. MACS, An Instrument, and a Methodology for Simultaneous and Global Measurements of the Coronal Electron Temperature and the Solar Wind Velocity on the Solar Corona, Thesis (PhD), University of Delaware, 6516
- Reginald, N. L., St. Cyr, O. C., Davila, J. M., Rabin, D. M., Guhathakurta, M., & Hassler, D. M. 2009, Electron-Temperature Maps of the Low Solar Corona: ISCORE Results from the Total Solar Eclipse of 29 March 2006 in Libya, *SoPh*, 260, 347
- Reginald, N. L., & Davila, J. M. 2000, MACS for Global Measurement of the Solar Wind Velocity and the Thermal Electron Temperature during the Total Solar Eclipse on 11 August 1999, *SoPh*, 195, 111
- St. Cyr, O. C., Plunkett, S. P., Michels, D. J., Paswaters, S. E., Koomen, M. J., Simnett, G. M., Thompson, B. J., Gurman, J. B., Schwenn, R., Webb, D. F., Hildner, E., & Lamy, P. L. 2000, Properties of Coronal Mass Ejections: SOHO LASCO Observations from January 1996 to June 1998, *J. Geophys. Res.*, 105(A8), 18
- Thernisien, A. 2010, Implementation of the Graduated Cylindrical Shell Model for the Three-Dimensional Reconstruction of Coronal Mass Ejections, *ApJS*, 194, 33
- Thernisien, A. F. R., Howard, R. A., & Vourlidas, A. 2006, Modeling of Flux Rope Coronal Mass Ejections, *ApJ*, 652, 763
- Tousey, R. 1973, "The solar corona", in *Space Research XIII, Proceedings of Open Meetings of Working Groups on Physical Sciences of the 15th Plenary Meeting of COSPAR*, Madrid, Spain, 10–24 May, 1972, Eds. Rycroft, M. J., & Runcorn, S. K. (Berlin: Akademie-Verlag), 713
- Yashiro, S., Gopalswamy, N., Michalek, G., St. Cyr, O. C., Plunkett, S. P., Rich, N. B., & Howard, R. A. 2004, A Catalog of White Light Coronal Mass Ejections Observed by the SOHO Spacecraft, *J. Geophys. Res.*, 109, A07105.